Electrochemical Behavior of Dysprosium in [EMIm]DCA Ionic Liquid Electrolyte

Kyong Mun Choe[1,*], Pyong Hun Kim[1], Gun Se Jo [1], Kum Hyok Choe[2], Chol Su Ri[3], Hyon Ho Ju[4]

[1]Institute of Analysis, Kim Chaek University of Technology, Pyongyang 950003, Democratic People's Republic of Korea

[2]School of Geoscience and Technology, Kim Chaek University of Technology, Pyongyang 950003, Democratic People's Republic of Korea

[3]Institute of Information Technology, High-Tech Research and Development Center, Kim Il Sung University, Pyongyang 950003, Democratic People's Republic of Korea

[4]School of Airspace science, Kim Il Sung University, Pyongyang 950003, Democratic People's Republic of Korea

**Corresponding Author, e-mail: ckm9313@163.com*

Telp: +86-17808055362

Abstract

The electrochemical behavior of dysprosium (Dy) in 1-ethyl-3-methylimidazolium dicyanamide ([EMIm]DCA) ionic liquid containing $DyCl_3$ was comprehensively studied using cyclic voltammetry (CV), chronoamperometry (CA), X-ray diffraction (XRD), scanning electron microscopy (SEM), and energy-dispersive X-ray spectroscopy (EDS). Cyclic voltammetric measurements revealed that the reduction of Dy^{3+} ions to metallic Dy is an irreversible process controlled by the diffusion of Dy^{3+} species, with an average charge transfer coefficient of 0.3898. Chronoamperometric data confirmed the one-step multielectron reduction mechanism of Dy^{3+} and the diffusion-controlled nature of the electrode process. The diffusion coefficient of Dy^{3+} calculated from CV measurements was determined to be 2.08×10^{-7} $cm^2 \cdot s^{-1}$, which is in good agreement with the value derived from CA curves. XRD analysis confirmed the formation of metallic Dy with a preferential orientation along the (002) crystallographic plane. SEM and EDS observations demonstrated the feasibility of

dysprosium electrodeposition in the [EMIm]DCA ionic liquid electrolyte, with the obtained deposits exhibiting a characteristic microgranular morphology.

Keywords:

Dysprosium; Electrodeposition; Ionic liquid; Cyclic voltammetry; Diffusion-controlled process

1. INTRODUCTION

Dysprosium (Dy), a member of the lanthanide series (rare earth elements, REEs), possesses unique magnetic, optical, and nuclear properties, making it indispensable in advanced technologies. It is widely used as an additive in neodymium-iron-boron (NdFeB) magnets to enhance high-temperature stability, as control rods in nuclear reactors, and in laser materials and phosphors [1, 2]. Despite its technological importance, the extraction and purification of Dy remain challenging due to its low natural abundance (≈1% in REE-bearing minerals such as bastnaesite and monazite) and dispersion in ores. Therefore, further research and improvement of Dy extraction techniques are necessary to develop more cost-effective and economically viable methods [3–13]. Recent research efforts aimed at addressing these issues have focused on studying the electrochemical and spectroscopic properties of Dy in its molten state [14, 15]. Investigations have been conducted on the electrodeposition of Dy in molten salt systems to synthesize various Dy intermetallic compounds [16]. The electrodeposition of rare earth metals and their alloys typically occurs in high-temperature molten salt environments [17, 18]. Additionally, studies have explored the use of liquid cathodes for electrodeposition processes, particularly for the electrowinning and electrorefining of rare earth elements, actinides, and titanium [19]. The use of a liquid cathode offers several advantages: (1) facilitated separation of electrolysis products due to the significant density difference between the electrolyte and the liquid cathode; (2) maintenance of a constant electrode surface area, ensuring parameter stability throughout the process; (3) prevention of irregular crystal growth, thereby reducing the required operating voltage due to the shortened cathode-anode distance; (4) enhanced coalescence of micro-drops and metallic fog; and (5) feasibility for continuous process design [20].

Ionic liquids (ILs) are emerging as promising electrolytes for energy storage devices due to their wide electrochemical windows, nonflammability, low volatility, and excellent thermal and chemical stability [21]. ILs are a class of solvents composed entirely of ions. For electrochemical deposition applications, two main families of ILs are predominantly used:

first-generation chloroaluminate ILs, and second-generation 'air- and water-stable' ILs with hydrophobic anions such as tetrafluoroborate, hexafluorophosphate, trifluoromethanesulfonate, or bis(trifluoromethylsulfonyl)imide. Notably, ILs based on weakly coordinating anions, including tetrafluoroborate (BF_4^-), hexafluorophosphate (PF_6^-), and bis(trifluoromethylsulfonyl)imide ($TFSI^-$), have limited ability to dissolve various metal salts, especially metal chloride salts [22, 23]. ILs are suitable for the electrodeposition of many metals and their alloys. Some researchers have investigated the IL-based electrodeposition of tin with different structural configurations as anodes for lithium-ion batteries, clarifying the differences in electrochemical behavior among three ILs: [EMIm]BF_4, [EMIm]TfO, and [EMIm]DCA [24]. ILs containing the dicyanamide (DCA^-) anion exhibit superior metal salt solubility due to their excellent coordination properties [25]. When 1-ethyl-3-methylimidazolium (EMIm) is used as the cation, the resulting IL typically has low viscosity and high electrical conductivity. The interactions between IL anions and metal ions significantly affect metal speciation and determine their solubility characteristics. A variety of ILs have been studied for the electrodeposition of rare earth metals and their alloys [26, 27]. A one-step electrodeposition method for the synthesis of silicon/terbium nanowires using ILs has been successfully demonstrated [28]. This deposition technique offers significant advantages over conventional methods due to its simplicity, cost-effectiveness, and avoidance of harsh deposition conditions. The intense room-temperature luminescence and millisecond-range lifetime of the electrodeposited nanowires confirm their high quality for applications in modern optoelectronic devices. The electrochemical co-deposition method described provides a simple and cost-effective alternative for the synthesis of rare earth-incorporated silicon nanostructures.

Additionally, some researchers have investigated the simultaneous electrodeposition of Dy and terbium (Tb) in [EMIm]BF_4 electrolyte [29]. Their results showed that the co-electrodeposition of Dy and Tb in [EMIm]BF_4 proceeds through an irreversible mechanism controlled by diffusion. The ILs 1-ethyl-3-methylimidazolium tetrafluoroborate ([EMIm]BF_4) and 1-ethyl-3-methylimidazolium dicyanamide ([EMIm]DCA) are characterized by lower costs compared to other ILs, while exhibiting extremely high ionic conductivities. Some researchers have studied the electrochemical behavior of Tb in [EMIm]BF_4 and [EMIm]DCA systems [30]. Their study showed that [EMIm]DCA is superior to [EMIm]BF_4 for Tb deposition.

Although several studies have examined the electrodeposition of rare earth elements and their alloys in [EMIm]DCA systems, research specifically focusing on the electrochemical behavior of Dy in [EMIm]DCA electrolytes remains limited. Therefore, the present study

comprehensively investigates the electrochemical behavior of Dy on platinum electrodes in $DyCl_3$–1-ethyl-3-methylimidazolium dicyanamide electrolytes, using a combination of electrochemical methods, XRD analysis, SEM, and EDS .

2. Experimental

2.1. Materials and Chemicals

1-Ethyl-3-methylimidazolium dicyanamide ([EMIm]DCA, 99%) was purchased from Lanzhou Greenchem ILs (China) and dried under vacuum at 373 K for 12 h to remove residual water. Anhydrous $DyCl_3$ (Aldrich, 99.9%) was dried at 473 K (200 °C) for 12 h in a vacuum desiccator to eliminate moisture. Platinum plates (Jinchuan Group Ltd, China, 0.5 cm^2) served as the working and counter electrodes, and a platinum wire (1.5 mm diameter) was used as the quasi-reference electrode. All materials were handled in an argon-filled glove box (UNILAB Pro SP, MBraun) with O_2 and H_2O contents below 1 ppm

2.2. Electrolysis Experiment

The electrolyte was prepared by dissolving 1.344 g (0.05 M) of anhydrous $DyCl_3$ in 100 mL of [EMIm]DCA at 333 K under magnetic stirring for 24 h, resulting in a homogeneous solution. After cooling, a 0.05 M $DyCl_3$ solution in [EMIm]DCA IL was prepared at room temperature. All electrochemical experiments were conducted in a glove box under a purified argon atmosphere using an HCP-803 electrochemical workstation (BioLogic) controlled by EC-Lab software. A 30 mL Teflon electrochemical cell with a three-electrode configuration was used. A platinum plate (S = 0.5 cm^2) served as the working electrode, another platinum plate (S = 0.5 cm^2) as the counter electrode, and a platinum wire (15 mm diameter) as the quasi-reference electrode. The platinum wire quasi-reference electrode was selected due to its sufficient electrochemical stability in the electrolytes throughout the experiment. The schematic diagram of this electrolysis experiment is shown in the Figure 1. All electrodes were polished with 0.3 μm alumina paste, sequentially cleaned with 1 M HNO_3, acetone, and deionized water, and finally vacuum-dried before use. All electrochemical experiments were conducted at room temperature (298 ± 2 K) without electrolyte agitation. After electrolysis, the cathode was removed from the electrolyte, rinsed thoroughly with ethanol, and the resulting deposits were dried in a vacuum desiccator for at least 2 h at room temperature. The mass loading of Dy electrodes obtained in [EMIm]DCA ILs at various cathodic potentials was extremely low.

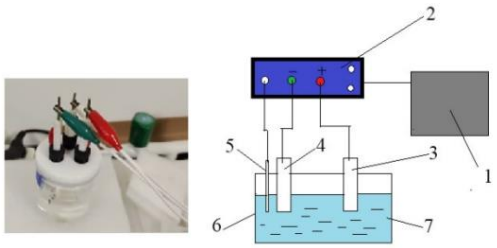

Figure. 1. The schematic diagram of the Electrolysis Experiment

1-computer, 2-electrochemical workstation, 3- counter electrode, 4- working electrode, 5-the quasi-reference electrode, 6- electrochemical cell, 7-electrolyte.

The crystalline structure of the deposits was analyzed by X-ray diffractometry (XRD, Bruker-AXS D8 Advance) using Cu Kα radiation at a scanning rate of 3° min^{-1}. The morphology of the electrodeposits was examined using a scanning electron microscope (JEOL6380LV) equipped with an energy-dispersive spectrometer.

3. Results and discussion

3.1. Reduction Process of Dy^{3+} in $DyCl_3$-[EMIM]DCA

To investigate the electrochemical behavior of Dy^{3+} in this IL, cyclic voltammograms (CVs) of 0.05 M $DyCl_3$ in [EMIm]DCA were recorded at different scan rates (10 to 50 mV s^{-1}) on a platinum electrode at room temperature, as shown in Figure 1. In Figure 1, the cathodic reduction peak potentials (E_{pc}) shift negatively with increasing scan rate, while the cathodic reduction current density (j_p) increases proportionally with the scan rate. The presence of a current loop during the cathodic scan indicates that the electrodeposition of Dy on the platinum electrode requires an overpotential to initiate nucleation and growth processes. As shown in Figure 1, the CV exhibits only a cathodic reduction peak for Dy^{3+}, with no corresponding anodic oxidation peak. According to previous experimental results [29], the reduction processes of both Tb^{3+} and Dy^{3+} ions in [EMIm]BF_4 electrolytes are irreversible, similarly lacking anodic oxidation peaks in their CVs. Furthermore, the literature findings revealed that the reduction of Dy^{3+} proceeds irreversibly in a single step. Therefore, by comparison with the literature [29], it can be concluded that the oxidation of Dy^{3+} cannot occur in IL electrolytes containing $DyCl_3$.

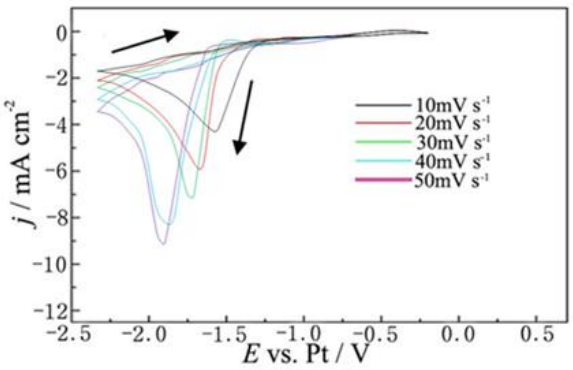

Figure. 1. Cyclic voltammograms of 0.05 M $DyCl_3$ in [EMIm]DCA on a platinum electrode with different scan rates at room temperature.

Furthermore, in the present study, when the potential was scanned in the positive direction, no anodic oxidation process of Dy was observed. This phenomenon is attributed to the formation of complexes between Cl^- and DCA^- anions with the $EMIm^+$ cation. Analysis of the CV curves suggests that the cathodic reduction process of Dy in these electrolytes is irreversible and occurs in a single step. As shown in Figure 1, the cathodic reduction peak potential of Dy^{3+} in [EMIm]DCA was determined to be 1.56 V (scan rate 10 mV s^{-1}). These findings indicate that Dy^{3+} species formed in the [EMIm]DCA electrolyte are relatively easy to reduce, suggesting that the speciation of Dy^{3+} dissolved in this electrolyte may differ significantly. Dy^{3+} cations in the [EMIm]DCA system are more likely to associate with both Cl^- and DCA^- anions to form complexes, facilitated by the strong coordinating ability of DCA^- toward Dy^{3+}. As reported in the literature [25], the viscosities of $[EMIm]BF_4$ and [EMIm]DCA are 377 cP (at 295 K) and 198 cP (at 301 K), respectively, indicating significant differences in viscosity between these solutions. Notably, the reduction peak current density of the Dy^{3+}/Dy couple in [EMIm]DCA IL is considerably high. The significantly lower viscosity of [EMIm]DCA leads to more efficient charge transfer and higher ionic conductivity. Consequently, the observed shift in the reduction peak potential of the Dy^{3+}/Dy couple in this system may also be attributed to differences in diffusion processes.

The difference between the cathodic peak and half-peak potentials ($|E_{pc} - E_{pc/2}|$) in this system increases significantly with increasing scan rate. At the lowest scan rate of 10 mV s^{-1}, the $|E_{pc} - E_{pc/2}|$ value for [EMIm]DCA at 298 K was determined to be 102.4 mV. This value is substantially higher than the 19mV threshold (at 298 K) characteristic of a reversible electrochemical process. This observation is primarily attributed to the resistive nature of organic electrolytes and the presence of uncompensated solution resistance in the CVs [31, 33].

Analysis of the CVs for Dy in this electrolyte suggests that the reduction of Dy^{3+} to Dy on the platinum electrode proceeds via an irreversible mechanism [32].

Furthermore, the strong linear relationships observed between the cathodic peak current densities (j_{pc}) and the square root of the scan rate ($v^{1/2}$), as shown in Figure 2, indicate that the reduction process of Dy^{3+} in this IL is diffusion-controlled. However, it is noteworthy that the plots of j_{pc} versus $v^{1/2}$ in this IL do not pass through the origin. The non-zero intercepts in these linear plots may be partially attributed to the significant influence of uncompensated electrolyte resistance, adsorption phenomena, and certain surface chemical coupled reactions [33].

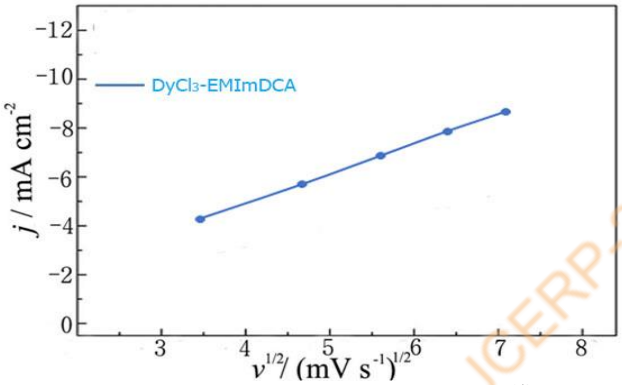

Figure. 2. Relationships between the j_{pc} and the $v^{1/2}$ obtained from Fig. 1.

For an irreversible one-step multielectron reaction process, the diffusion coefficient of Dy^{3+} can be calculated using the irreversible Randles–Sevcik equation (1) [32]:

$$i_{pc} = 0.4958nFAC_{Dy^{3+}}D_{Dy^{3+}}^{1/2}(\frac{\alpha n_{\alpha}Fv}{RT})^{1/2} \qquad (1)$$

where i_{pc} is the cathodic peak current, n is the number of transferred electrons, F is the Faraday constant, A is the working electrode area, $C_{Dy^{3+}}$ is the concentration of Dy^{3+} species, $D_{Dy^{3+}}$ is the diffusion coefficient of Dy^{3+} species, α is the transfer coefficient, ν is the scan rate, R is the gas constant, and T is the absolute temperature. The αnα value can be calculated using equation (2) [32]:

$$\left|E_{pc} - E_{\frac{pc}{2}}\right| = \frac{1.857RT}{\alpha nF} \qquad (2)$$

where E_{pc} is the cathodic peak potential, $E_{pc/2}$ is the cathodic half-peak potential, α is the electron transfer coefficient, n is the number of electrons, and F is the Faraday constant. The $\alpha_{n\alpha}$ values for the [EMIm]DCA IL at 298 K were calculated using equation (2) and the data from Figure 1, with the results shown in Table 1. The average value of $\alpha_{n\alpha}$ ($n\alpha$ = 3) was calculated to be 0.398. Substituting the αnα value and other parameters into equation (1), the diffusion coefficient of Dy^{3+} species in [EMIm]DCA at 298 K was determined to be

approximately 2.08 × 10^{-7} cm^2/s. Notably, the diffusion coefficient of Dy^{3+} species in [EMIm]DCA IL is substantially large.

Table 1. Data of cyclic voltammogram with various potential scan rates in [EMIm]DCA

v/mV·s^{-1}	j_{pc}/mAcm^{-2}	E_{pc}/V	$\lvert E_p - E_{pc/2}\rvert$/mV	α
10	4.08	-1.56	102.8	0.463
20	5.61	-1.60	110.1	0.433
30	6.87	-1.66	124.1	0.384
40	7.95	-1.72	136.6	0.349
50	8.82	-1.85	148.6	0.320
Average				0.3898

This observation suggests that the relatively enhanced mobility of Dy^{3+} species in the [EMIm]DCA system is likely associated with the lower viscosity of [EMIm]DCA and the favorable coordination interactions between the solution components and Dy^{3+} ions at the electrode interface.

3.2. Electrodeposition of Dy^{3+} in $DyCl_3$–[EMIm]DCA and Characterization of Dysprosium Electrodeposits

To investigate the effects of cathodic potential and IL anion type on the characteristics of Dy electrodeposits, potentiostatic electrodeposition experiments were conducted on platinum electrodes in quiescent electrolytes at room temperature. For the 0.05 M $DyCl_3$–[EMIm]DCA system, electrodeposition was performed at potentials of –1.6, –1.7, –1.8, and −1.9 V versus platinum for 30 minutes. The onset electrodeposition potential of –1.6 V (for [EMIm]DCA) was selected based on the respective reduction peak potentials of Dy determined from CV measurements (Figure 1). The current density-time curves recorded during the electrodeposition of Dy in these ILs at different cathodic potentials and room temperature are shown in Figure 3. As illustrated in Figure 3, the current density increases significantly with the application of more negative potentials. However, the current densities reach a plateau and remain relatively stable during the electrodeposition process, indicating the formation of compact electrodeposits. The reduction current decreases rapidly within a very short time and then stabilizes over longer periods.

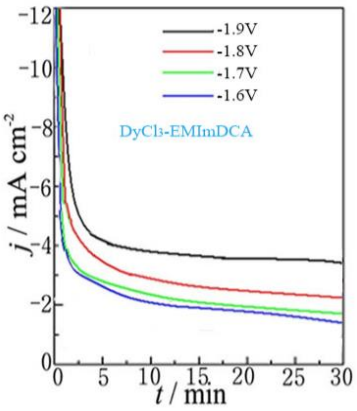

Figure. 3. Variation of current density with time during the electrodeposition of Dy from 0.05 M $DyCl_3$ in [EMIm]DCA.

This initial rapid decrease in reduction current is attributed to the formation of an electric double layer around the electrodes, while the subsequent stabilization over longer times results from the development of new diffusion layers around the already formed crystal nuclei. Consequently, the rate-determining step of the electrode process is diffusion-controlled [29].

As is well-known, the unsteady-state limiting diffusion current at any time can be expressed by equation (3) [31]:

$$i = \frac{nFAC_{Dy^{3+}}D_{Dy^{3+}}^{1/2}}{t^{1/2}\pi^{1/2}} \qquad (3)$$

where i is the cathodic current, n is the number of transferred electrons, F is the Faraday constant, A is the working electrode area, $C_{Dy^{3+}}$ is the concentration of Dy^{3+} species, $D_{Dy^{3+}}$ is the diffusion coefficient of Dy^{3+} species, t is the time during cathodic current flow, and π is 3.14. Using equation (3), the diffusion coefficient for the [EMIm]DCA IL electrolyte was calculated to be 1.48×10^{-7} cm^2/s, which is in good agreement with the diffusion coefficient derived from the CV curves. These consistent results strongly suggest that the electrochemical reduction process of Dy in these electrolytes is governed by a diffusion rate-determining step.

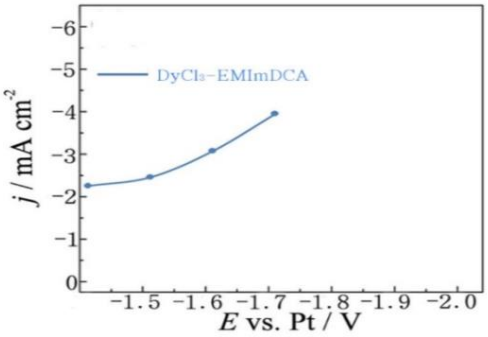

Figure. 4. Variation of average current density with different potentials in 0.05 M $DyCl_3$ of [EMIm]DCA at room temperature for 30 min.

Figure 4 shows the influence of cathodic potential on the average current density in these electrolytes. The cathodic reduction current density increases with more negative potentials. Furthermore, the current densities recorded in [EMIm]DCA IL at different cathodic potentials are notably high. This phenomenon may be attributed to the lower viscosity and more efficient charge-transfer characteristics of [EMIm]DCA IL.

To confirm the formation of metallic Dy, XRD analysis was performed on the Dy electrodeposits obtained from this IL system. The XRD patterns of Dy electrodeposits obtained on a platinum electrode in these electrolytes at different cathodic potentials and room temperature for 30 minutes are shown in Figure 5.

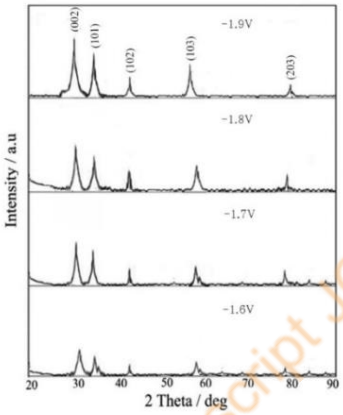

Figure. 5. XRD patterns of the deposits in 0.05 M $DyCl_3$ of [EMIm]DCA at different potentials for 30 min.

For the Dy electrodeposits obtained in [EMIm]DCA ILs (Figure 5) at the four selected cathodic potentials, the XRD patterns show a dominant diffraction peak at 32.78°, indicating that the Dy electrodeposits have a preferential orientation along the (002) plane. According to literature data [29], the XRD patterns of metallic Dy are consistent with PDF015-0430 (Hexagonal) of Dy from the XRD PDF database. As shown in Figure 5, the relative intensity of the XRD patterns obtained from [EMIm]DCA is significantly high. This observation is attributed to the different coordination abilities of the anions toward Dy^{3+} ions on the electrode surface and the lower viscosity of [EMIm]DCA. These XRD results are consistent with the aforementioned electrochemical experimental findings [29], confirming that the nucleation and growth of Dy on the platinum electrode may be accelerated with increasing cathodic potential. The confirmation of metallic Dy through XRD analysis supports the irreversible nature of the Dy reduction process in this electrolyte.

The morphology, structure, and shape of the resulting electrodeposits were examined by SEM with EDS analysis, which confirmed the presence of Dy, indicating its reduction.The Dy electrodeposit and corresponding EDS analysis are presented in Figure 6.

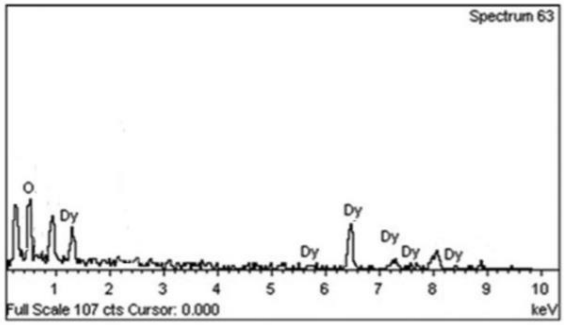

Figure. 6. EDS spectra of deposits in 0.05 M $DyCl_3$ of [EMIm]DCA at -1.9 V for 30 min.

As shown in Figure 6, the presence of oxygen is attributed to the immediate oxidation of the electrodeposited metal. The electrolyte is hydrophobic, so it cannot be removed from the electrode by simple rinsing with water. To remove the electrolyte, the electrode should be rinsed with acetone or another polar organic solvent, but this leads to the immediate oxidation of the electrodeposited metal, accompanied by increased oxygen concentrations in the EDS analysis and the formation of a white layer on the electrode surface.

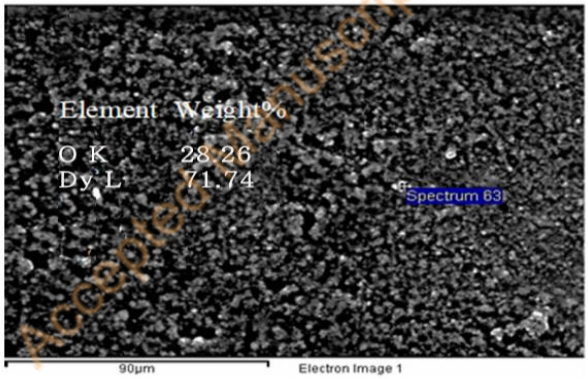

Figure. 7. SEM images of deposits in 0.05 M $DyCl_3$ of [EMIm]DCA at -1.9V for 30 min.

The EDS spectra confirmed the successful reduction of Dy in this electrolyte, which is consistent with the XRD results. The Dy electrodeposit in [EMIm]DCA was microgranular with distinct particles in the range of 1–5 µm. From Figure 7, the nucleation and growth process of Dy in this electrolyte is clearly visible. The SEM images confirm the results of the potentiostatic electrodeposition experiments.

4. CONCLUSIONS

This study comprehensively investigated the electrodeposition of Dy in [EMIm]DCA IL. The voltammetric behavior of the electrochemical processes of Dy was systematically studied. CV results showed that the reduction process of Dy in this electrolyte is an irreversible one-step multielectron reaction, with an average transfer coefficient of Dy^{3+} of approximately 0.398. The diffusion coefficient of Dy^{3+} species in [EMIm]DCA at 298 K is 2.08×10^{-7} cm^2/s, confirming that the electrodeposition process of Dy in this electrolyte is diffusion-controlled. The enhanced mobility of Dy^{3+} species in [EMIm]DCA is likely related to the low viscosity of the IL and the good coordination between the solution and Dy^{3+} ions at the electrode. Chronoamperometric results confirmed that the reduction process of Dy is diffusion-controlled. XRD patterns of Dy deposits show that metallic Dy is obtained during electrodeposition, and the crystallographic orientation of the Dy electrodeposits is significantly influenced by the electrolyte anion and electrodeposition potential. EDS spectra confirmed the successful reduction of Dy in this electrolyte. [EMIm]DCA is recommended as a superior electrolyte for efficient Dy electrodeposition.

Graphical Abstract

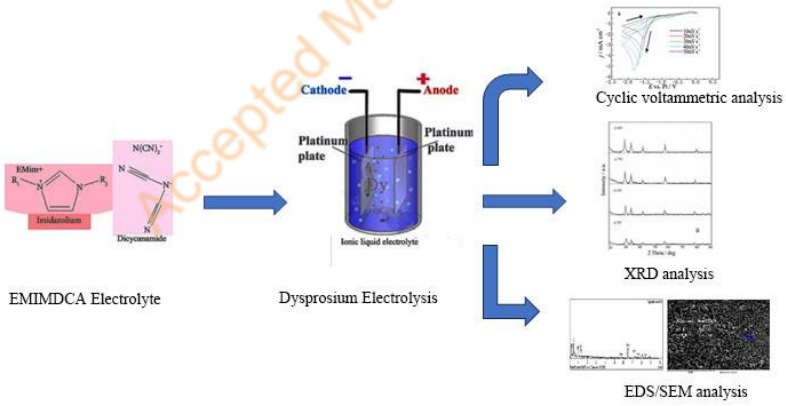

Acknowledgements

The authors gratefully acknowledge Professors Zhai Yu Chun and Hong Shong Chol for their assistance with electrochemical experiments and XRD, SEM, EDS analyses, respectively.

CRediT Author Statement

Author Contributions: *Kyong-Mun Choe*: Conceptualization, Methodology, Investigation, Resources, Data Curation, Writing, Review and Editing, Supervision; *Pyong-Hun Kim*: Conceptualization, Methodology, Formal Analysis, Data Curation, Writting Draft Preparation, Visualization, Software, Project Administration; *Gun-Se Jo and Hyon-Ho Ju*: Validation, Writing, Review and Editing, Data Curation; *Kum-Hyok Choe* and *Chol-Su Ri*: Investigation, Resources, Writing, Review and Editing, Validation. All authors have read and agreed to the published version of the manuscript.

References

[1] Krishnamurthy, N., & Gupta, C. K. (2015). Extractive Metallurgy of Rare Earths (2nd ed.). Boca Raton: CRC Press (Taylor & Francis). https://doi.org/10.1201/b19055

[2] Wübbeke, J. (2013). Rare Earth Elements in China: Policies and Narratives of Reinventing an Industry. *Resources Policy*, 38(3), 384–394. https://doi.org/10.1016/j.resourpol.2013.05.005

[3] Attia, Y. A. (1990). Extraction and Refining of High Purity Terbium Metal From Rare Earth Resources. *Mineral Processing and Extractive Metallurgy Review*, 7(2), 95–114. https://doi.org/10.1080/08827509008952668

[4] Zhang, Q. B., Hua, Y. X., Xu, C. Y., Li, Y., Li, J., & Dong, P. (2015). Non-haloaluminate ionic liquids for low-temperature electrodeposition of rare-earth metals—A review. *Journal of Rare Earths*, 33(10), 1017–1025. https://doi.org/10.1016/S1002-0721(14)60520-2

[5] Sasireka, D., Kavitha, N., Kumar, T. S., & Chandrasekar, L. B. (2025). Effect of dysprosium concentration on the photocatalytic and electrochemical properties of zirconium ferrite nanoparticles. *Journal of Crystal Growth*, 671, 128354. https://doi.org/10.1016/j.jcrysgro.2025.128354

[6] Abdou, N. Y., Alazab, H. A., & Sadek, A. M. (2026). Eco-friendly synthesis of dysprosium-doped nano-hydroxyapatite using sea-shells: A study in thermoluminescence. *Applied Radiation and Isotopes*, 227, 112279. https://doi.org/10.1016/j.apradiso.2025.112279

[7] Murugan, D., Kumar, A., Dhayalan, A., & Kanan, S. (2025). Tough-engineered multifunctional alendronate anchoring of dysprosium impregnated luminescent polyvinyl alcohol-chitos

an composite hydrogels. *Biomaterials Advances*, 177, 214406. https://doi.org/10.1016/j.bioadv.2025.214406

[8] El Kinawy, M., Farag, M. M., El Faramawy, N., & Abdou, N. Y. (2025). Impact of dysprosium doping concentration on the thermoluminescence properties of tricalcium phosphate. *Journal of Luminescence*, 287, 121475. https://doi.org/10.1016/j.jlumin.2025.121475

[9] Yang, F., Duan, Y. L., Xie, J. N., Wang, H. L., Lu, G. J., & Zhou, H. H. (2025). Anion-manipulated coordination-catalyzed tandem reaction to construct multinuclear dysprosium-based single-molecule magnets. *Journal of Molecular Structure*, 1342, 142721. https://doi.org/10.1016/j.molstruc.2025.142721

[10] Senthilkumar, D., Kuo, C. Y., Albassami, N. A., & Mani, G. (2025). Tailored electrochemical sensing of phenolic pollutant via dysprosium molybdate-infused multi-walled carbon nanotubes for superior detection performance. *Journal of Water Process Engineering*, 79, 109002. https://doi.org/10.1016/j.jwpe.2025.109002

[11] Bissengaliyeva, M. R., Bespyatov, M. A., Gogol, D. B., Taimassova, S. T., & Sadyrbekov, D. T. (2025). Magnetic properties, thermodynamic functions and Schottky contributions to the heat capacity of terbium, dysprosium, holmium, ytterbium titanates. *Journal of Alloys and Compounds*, 1044, 184289. https://doi.org/10.1016/j.jallcom.2025.184289

[12] Ahmad, A. U., Yam, F. K., & Ghoshal, S. K. (2025). Correlation of tunable Dy^{3+} environments with physical and optical properties of dysprosium-activated borate glass: Effect of gold and silver nanoparticles. *Next Research*, 2(1), 100186. https://doi.org/10.1016/j.nexres.2025.100186

[13] Yang, X. D., Luo, H. Q., Zhou, J. F., Sun, P. K., Guo, Y. X., & Zhao, J., et al. (2025). Ball-milled dysprosium oxide loaded biochar-montmorillonite composite for efficient removal and great recycling performance of cationic organic pollutants. *Industrial Crops and Products*, 235, 121777. https://doi.org/10.1016/j.indcrop.2025.121777

[14] Bermejo, M. R., Gómez, J., Martinez, A. M., Barrado, E., & Castrillejo, Y. (2008). Electrochemistry of terbium in the eutectic LiCl–KCl. *Electrochimica Acta*, 53, 5106–5112. https://doi.org/10.1016/j.electacta.2008.02.058

[15] Nadar, N. R., Deepak, J., Sharma, S. C., RadhaKrushna, B. R., Akila, K., & Anitha, R. (2025). Novel scandium-doped cobalt chromate: Dopamine sensing and superior supercapacitor

performance. *Materials Science and Engineering: B*, 321, 118306. https://doi.org/10.1016/j.mseb.2025.118306

[16] Tugce, A. G., Ayse, Y., & Borte, M. K. (2025). Advances in electrochemical methods for rare earth elements recovery: A comprehensive review. *Process Safety and Environmental Protection*, 196, 106897. https://doi.org/10.1016/j.psep.2025.106897

[17] Tai, Q. Y., Yun, X., Yan, Y. D., Ma, Z. C., Ma, F. Q., & Zhang, M. L., et al. (2021). Recovery and separation of rare earth elements by molten salt electrolysis. *International Journal of Minerals, Metallurgy and Materials*, 28(6), 899–908. https://doi.org/10.1007/s12613-020-2228-4

[18] Bourbos, E., Giannopoulou, I., Karantonis, A., Paspaliaris, I., & Pania, D. (2016). Electrodeposition of rare earth metals from ionic liquids. In *Rare Earths Industry* (pp. 199–207). https://doi.org/10.1016/B978-0-12-802328-0.00013-9

[19] Abbasalizadeh, A., Malfliet, A., Seetharaman, S., Sietsma, J., & Yang, Y. X. (2017). Electrochemical extraction of rare earths from molten fluorides. *Journal of Sustainable Metallurgy*, 3, 627–637. https://doi.org/10.1007/s40831-017-0120-x

[20] Molodkina, E. B., Ehrenburg, M. R., & Rudnev, A. V. (2022). Electrochemical Codeposition of Sm and Co in a Dicyanamide Ionic Liquid. *Russian Journal of Electrochemistry*, 58, 1083–1093. https://doi.org/10.1134/S1023193522120059

[21] Rajyashree, L., & Ramana, G. R. (2023). Rare Earth and Critical Base Metals Electrodeposition Using Urea-Choline Chloride Ionic Liquids. In *The Minerals, Metals & Materials Series* (pp. 1151–1159). https://doi.org/10.1007/978-3-031-22765-3_15

[22] Zhou, J., Meng, X. H., Zhang, R., Liu, H. Y., & Liu, Z. C. (2021). Progress on Electrodeposition of Rare Earth Metals and Their Alloys. *Electrocatalysis*, 12, 628–640. https://doi.org/10.1007/s12678-021-00688-1

[23] Rudnik, E. (2026). From Electrolyte to Alloys: Electrodeposition of Rare Earth Element-Based Thin Films—State of the Art. *Materials*, 19(7), 1350. https://doi.org/10.3390/ma19071350

[24] Makarova, I., Soboleva, E., Osipenko, M., Kurilo, I., Laatikainen, M., & Repo, E. (2020). Electrochemical leaching of rare-earth elements from spent magnets. *Hydrometallurgy*, 192, 105264. https://doi.org/10.1016/j.hydromet.2020.105264

[25] Yuan, Y. T., Luo, H. M., & Dai, S. (2025). Electrodeposition of Rare Earth Elements Using Ionic Liquids for Energy-Efficient Recovery. *Journal of The Electrochemical Society*, 2, 2849. https://doi.org/10.1149/MA2025-02612849

[26] Thomas, S., Mallet, J., Bahuleyan, B. K., & Molinari, M. (2020). Growth of homogeneous luminescent silicon-terbium nanowires by one-step electrodeposition in ionic liquids. *Nanomaterials*, 10, 2390. https://doi.org/10.3390/nano10172390

[27] Zhang, Y., & Chen, J. (2019). Preparation of $REPO_4$ (RE-La–Gd) nanorods from an ionic liquid extraction system and luminescent properties of $CePO_4:Tb^{3+}$. *Rare Metals*, 38, 122–128. https://doi.org/10.1007/s12598-016-0701-z

[28] Zhang, Y., & Chen, J. (2015). Controllable preparation of $CeF_3:Tb^{3+}$ nanostructures with different morphologies from an ionic liquid-based extraction system. *Colloids and Surfaces A: Physicochemical and Engineering Aspects*, 470, 130–137. https://doi.org/10.1016/j.colsurfa.2015.01.076

[29] An, H. S., Kim, P. H., & Yu, N. C. (2023). Simultaneous electrodeposition behavior of dysprosium and terbium in 1-ethyl-3-methyl-imidazolium tetrafluoroborate ionic liquid. *Journal of the Indian Chemical Society*, 100(7), 100097. https://doi.org/10.1016/j.jics.2023.100972

[30] Choe, K. M., Kim, P. H., & Yu, N. C. (2025). Electrochemical behaviors of terbium from $TbCl_3$-$EMImBF_4$ and $TbCl_3$-EMImDCA ionic liquid electrolytes: a comparative study. *Journal of Solid State Electrochemistry*, 29, 2925–2934. https://doi.org/10.1007/s10008-024-06179-9

[31] Protsenko, V. S., Shaiderov, D. A., Butyrina, T. E., & Frolova, L. A. (2026). Electrodeposition of rare earth metals from deep eutectic solvents. *Journal of Solid State Electrochemistry*, 26, 6586–6595. https://doi.org/10.1007/s10008-026-06586-0

[32] Bard, A. J., & Faulkner, L. R. (2022). *Electrochemical Methods: Fundamentals and Applications*. New York: John Wiley & Sons. ISBN: 978-1-119-33405-7

[33] Bentley, C. L., Bond, A. M., Hollenkamp, A. F., Mahon, P. J., & Zhang, J. (2013). Advantages Available in the Application of the Semi-Integral Electroanalysis Technique for the Determination of Diffusion Coefficients in the Highly Viscous Ionic Liquid 1-Methyl-3-Octylimidazolium Hexafluorophosphate. *Analytical Chemistry*, 85(4), 2239–2245. https://doi.org/10.1021/ac303042r

FIGURE CAPTIONS

Figure. 1. Cyclic voltammograms of 0.05 M $DyCl_3$ in [EMIm]DCA on a platinum electrode with different scan rates at room temperature

Figure. 2. Relationships between the j_{pc} and the $v^{1/2}$ obtained from Fig. 1.

Figure. 3. Variation of current density with time during the electrodeposition of Dy from 0.05 M $DyCl_3$ in [EMIm]DCA.

Figure. 4. Variation of average current density with different potentials in 0.05 M $DyCl_3$ of [EMIm]DCA at room temperature for 30 min.

Figure. 5. XRD patterns of the deposits in 0.05 M $DyCl_3$ of [EMIm]DCA at different potentials for 30 min.

Figure. 6. EDS spectra of deposits in 0.05 M $DyCl_3$ of [EMIm]DCA at -1.9 V for 30 min.

Figure. 7. SEM images of deposits in 0.05 M $DyCl_3$ of [EMIm]DCA at -1.9V for 30 min.

TABLE CAPTIONS

Table 2. Data of cyclic voltammogram with various potential scan rates in [EMIm]DCA